Geoscience Frontiers 14 (2023) 101512

HOSTED BY

Contents lists available at ScienceDirect

Geoscience Frontiers

journal homepage: www.elsevier.com/locate/gsf

Research Paper

Sticking together: Mechanisms of quartz synneusis in high-silica magma

Brendan Dyck

Department of Earth, Environmental and Geographic Sciences, The University of British Columbia, 4237 University Way, Kelowna, BC V1V 1V7, Canada

ARTICLE INFO

Article history:
Received 22 August 2022
Revised 24 October 2022
Accepted 15 November 2022
Available online 19 November 2022
Handling Editor: Richard Palin

Keywords:
Synneusis
Granite
Magmatic behaviour
EBSD
Cathodoluminescence
Quartz

ABSTRACT

The formation of crystal clusters by synneusis (magmatic sintering) affects a wide range of magmatic systems from olivine clusters in komatiite to quartz clusters in high-silica granite. A common feature of synneusis in any mineral phase is the alignment of neighbouring crystals in certain lower-energy orientation relationships. However, the underlying mechanisms involved with both the alignment of crystals in lower-energy orientations and the binding of crystal clusters are not well understood. In the absence of mechanisms that bind crystals together upon contact, the same hydrodynamic forces that may bring crystals together can in theory also serve to disaggregate clusters. Here I use cathodoluminescence imaging and crystal orientation data from quartz clusters in high-silica granite to show that i) rapid crystalline neck growth along attachment surfaces and ii) grain rotation are two mechanisms that reduce the grain boundary energy of crystal clusters while increasing clusters' shear strength. The continued crystallization of sintered phases as the magmatic body cools further cements crystal pairs and resists cluster disaggregation. Together these mechanisms underpin both the formation and preservation of large crystal clusters in dynamic magmatic environments.

1. Introduction

The clustering of crystals in magmatic systems can significantly influence the mechanical behaviour of those systems (Bergantz and Ni, 1999; Jerram et al., 2003; McIntire et al., 2019). While there are multiple ways to form crystal clusters (e.g., epitaxial nucleation, twinning, dendritic growth) one of the primary mechanisms that operates in magmatic systems is synneusis – the attachment (or sintering) of previously isolated crystals suspended in a fluid environment (Vance, 1969). The products of synneusis of silicate minerals in crystal-poor and magma-rich bodies have been documented in a range of magmatic compositions that include olivine clusters in komatiite (e.g., Jerram et al., 2003) and basalt (e.g., Wieser et al., 2019), plagioclase clusters in intermediate compositions (e.g., Gogoi and Saikia, 2018; Zhu et al., 2018) and quartz clusters in high-silica granite (e.g., Beane and Wiebe, 2012; Dyck and Holness, 2022).

A common observation made on clusters formed by synneusis is the alignment of neighbouring crystals in certain lower-energy orientation relationships called coincident site lattices (CSL; Vance and Gilreath, 1967). Within the context of magmatic systems, the underlying mechanisms involved with both the alignment of and the binding of sintered crystals in CSL orientation relationships are not well understood. In a dynamic fluid environment, where crystals are able to move independently of each other, the fluid drag and attendant torque exerted on crystals may be orders of magnitude larger than the cohesive forces that hold the crystals together (Oyegbile et al., 2016). As such, in the absence of a mechanism to bind crystals together upon contact, the same hydrodynamic forces that may bring crystals together can in theory also serve to disaggregate clusters.

In this contribution I use electron backscatter diffraction (EBSD) and cathodoluminescence (CL) to document both the frequency of quartz crystal pair orientation relationships and the intracrystalline microstructural modification associated with the formation of quartz clusters from the high-silica Bobbenjaankop granite sill in South Africa. With these data, I explore the roles of i) rapid crystalline neck growth along synneusis contact planes, and ii) grain boundary energy-driven crystal rotation as mechanisms that may help bind quartz crystals together in CSL orientation relationships. Crystalline neck growth and grain rotation are both well-documented phenomena associated with the sintering of metal alloys and ceramics (Braginsky et al., 2005; Chaim, 2012; Dake et al., 2016; Bouala et al., 2017; Kini and Chokshi, 2020) that have so far received little attention in the study of mineral systems. However, both mechanisms appear to be key to the formation and preservation of large crystal clusters in dynamic magmatic environments. The approach taken in this study addresses one of the main challenges faced when studying the record of synneusis

E-mail address: Brendan.dyck@ubc.ca

https://doi.org/10.1016/j.gsf.2022.101512

in magmatic systems, which is that in a fully crystallized plutonic rock the intermediary crystal necks formed between sintered grains are not as readily observable as they are in crystal/liquid (or quenched glass) mixtures.

2. Material and methods

This study focuses on clusters of quartz crystals in a matrix of interstitial feldspar, biotite, and cassiterite found in samples collected from the Bobbenjaankop high-silica granite sill in South Africa (24°03′40″S, 28°45′30″E). The Bobbejaankop sill is a ~300-m-thick tabular, sub-horizontal intrusion of high-silica granite (>70 wt.% SiO_2) that belongs to the ca. 2.05 Ga A-type Lebowa Granite Suite of the Bushveld Complex (Walraven, 1993; Robb et al., 2000; Nazari-Dehkordi and Robb, 2022). Recent studies on the microstructure of quartz clusters and chemistry of zircon collected across the Bobbejaankop sill independently conclude the intrusion underwent closed-system fractionation and centripetal crystallization with quartz being the first major phase to crystallize from the magma (Gardiner et al., 2021; Dyck and Holness, 2022) during the initial stages of magmatic solidification when low crystal fractions of quartz (≤0.1) were suspended in a magma-rich and crystal-poor environment. As such, the quartz microstructures in this intrusion provide an opportunity to study the dynamics of synneusis and mineral growth.

2.1. Cathodoluminescence imaging

In an effort to identify microstructural modifications associated with quartz synneusis, six samples, collected along a vertical transect of the Bobbejaankop sill, were prepared for scanning electron microscope (SEM) cathodoluminescence (CL) imaging. Variation in the CL response of magmatic quartz can preserve a high-fidelity record of oscillatory growth zoning. It can also record a variety of microstructural modifications that manifest as changes to the regularity of growth zoning (e.g., truncation of internal zoning patterns, changes in the curvature of internal zonation, variation in the width of annuli). Two thin sections per sample were cut at orthogonal angles so as to cross-section clusters both parallel to and perpendicular to their long axes. CL images were generated on a FEI Quanta 650 SEM at the Department of Earth Sciences, University of Oxford. CL acquisition of entire thin-sections was performed under high-vacuum with an accelerating voltage of 20 kV, a working distance of 12.5 mm and 80 μs dwell-time, resulting in a montage of individual frames with half-field widths of ~2.0 mm and resolvable pixel widths of ~2.5 μm.

2.2. Crystal orientation mapping

The size and number density of clustered quartz grains increases towards the centre of the Bobbejaankop sill, with the largest clusters also containing the largest quartz grains found across the transect (Dyck and Holness, 2022). Accordingly, two samples from the centre of the sill with the largest quartz clusters were selected for crystal orientation mapping. Quartz crystal orientation data were collected by electron backscatter diffraction (EBSD) using a NordlysMax detector mounted to the same scanning electron microscope. EBSD data were acquired under low-vacuum mode with 50 Pa water vapour to prevent surface charging at the higher accelerating voltage of 30 kV. A working distance of 15 mm and a step-size of 20 μm were used for all EBSD analyses. The angular resolution of individual absolute crystal orientation measurements under these operating conditions is expected to be 0.1°–0.5° (Ruggles et al., 2016). All processing and plotting of EBSD data were carried out using the MTEX toolbox in Matlab (Bachmann et al., 2010). Mean orientations were calculated for each grain following the procedure outlined in Dyck and Holness (2022). Not only does this procedure account for any lattice distortion caused by the transition from hexagonal (high) to trigonal (low) quartz, it also avoids the minor effect of differential strain imposed on quartz during cooling (Beane and Wiebe, 2012). Minimum misorientation angles for grain boundaries were set at 10° and at 2° for subgrain boundaries (Hansen and Warren, 2015). Quartz-quartz pairs separated by 60° about the c-axis (Dauphine twin law) were identified and treated as single grains to account for common growth twinning. Processed orientation maps were then used to investigate the orientation relationship between all quartz-quartz pairs.

The six most common CSL orientation relationships observed in typical magmatic bihexagonal pyramidal quartz pairs, as described by the angle formed (misorientation) between the c-axes of the two crystals and the crystal face on which they meet, are: parallel rhomb, parallel prism, rhomb 90°, prism 90°, rhomb 27° (Esterel twin law), and s-face 90° (Fig. 1). Crystal orientation data were used to identify rhomb 90°, prism 90°, Esterel, and s-face 90° CSL orientation relationships. This was done by defining and plotting CSL boundaries using the *angle* and *rotation* functions in MTEX (e.g., 90° about [−1 1 1] for rhomb 90°; see Supplementary Material). Parallel CSL orientation relationships were recognised by overlaying CL images and identifying neighbouring grains with concentric oscillatory zoning that shared a common orientation. Without 3-D crystal data it was not possible to distinguish parallel crystals that meet on rhomb versus prism faces. Accordingly, both parallel orientations are combined in the data reported here. Combing these data will have no bearing on the conclusions as there should be no grain boundary energy difference between two parallel configurations.

3. Results

3.1. Orientation relationships of crystals in quartz clusters

In most of the previous studies that have looked at orientation relationships of crystals formed by synneusis, grain boundaries

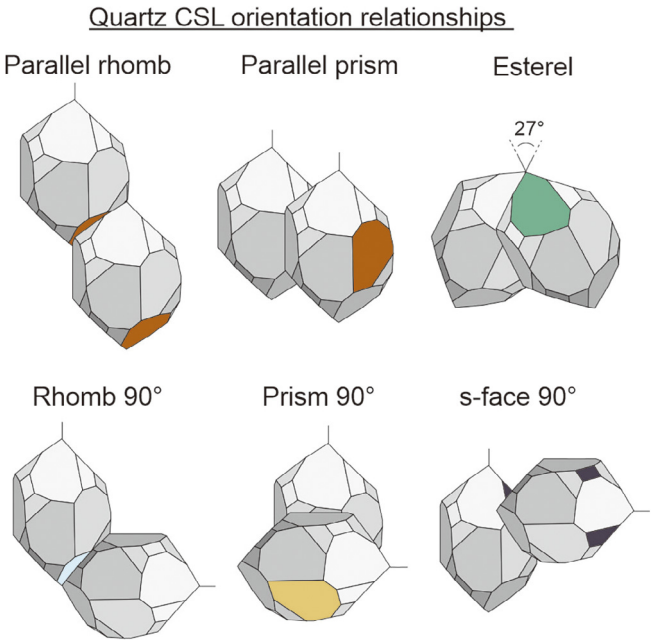

Fig. 1. Common coincident site lattice (CSL) orientation relationships for bihexagonal pyramidal quartz crystals.

that form CSL orientation relationships are identified by a misorientation with a defined rotation axis and angle (e.g., 90° ± 10° rotation about the 1101 axis for rhomb 90°; Wieser et al., 2019; Dyck and Holness, 2022). This approach detects crystal pairs with shared grain boundaries that are within a defined degree of rotation from CSL (e.g., ±10°), but does not quantify the frequency of pairs occurring at varying rotation angles from CSL. To evaluate how the alignment of crystals influences the likelihood of a pair being formed, I generated multiple orientation maps for each sample that characterized the orientation relationships of all grain boundary segments with varying degree of rotation from CSL (±10°, 20°, 30°, and 40°). On each map, the quartz–quartz grain boundaries that match the orientation relationships for rhomb 90°, prism 90°, and Esterel, and S-face 90° are coloured accordingly (Supplementary Material). I then labelled each pair of quartz grains and, with increasing rotation from the ideal coincident site lattice relationship, recorded the angle (e.g., <10°, 10°–20°, 20°–30°, and 30°–40°) at which a CSL orientation relationship was first identified for a pair (Supplementary Material). Because some grain boundaries can be classified as more than one CSL when the definition of CSL is relaxed (i.e., higher rotation angle), I only recorded the first CSL identified for each grain boundary segment as the rotation angle was increased.

Fig. 2 shows the distribution of total misorienation angles for all quartz-quartz pairs studied as well as the simulated distribution of uncorrelated grains with the same orientations as those measured. In both samples, there is a high frequency of non-random parallel, prism 90°, and rhomb 90° orientation relationships, which itself is a hallmark of clusters that were formed by synneusis (Vance, 1969). Fig. 3 displays the frequency of quartz–quartz pairs as a function of their angular rotation from the ideal CSL orientation relationships. The most common orientation relationships found in the Bobbejaankop quartz clusters are the parallel and 90° rotation of grains that meet along the prism and rhomb faces. In both samples it is generally the case that with increasing degree of rotation from the CSL orientation relationships there are fewer quartz pairs formed. 70% of all pairs in sample ZP131 and 62% of all pairs in sample BBK1 are recorded to be within 20° of rotation from one of the prism or rhomb CSLs. However, crystal pairs that form rhomb 90° and Esterel orientation relationships occur most frequently in both samples at 10°–20° from CSL. For pairs attached about the s-face 90° CSL there also appears to be a slight increase in the likelihood of synneusis with increasing rotation from CSL. However, there are too few quartz pairs that match the orientation criteria for s-face 90°, only ~6% (n = 7) of quartz pairs in sample ZP131 and ~13% (n = 25) in sample BBK1 can be defined within 40° of rotation from the s-face 90° CSL, to draw conclusions from this trend.

3.2. Quartz cathodoluminescence zoning patterns

The majority of quartz grains in all of the samples examined exhibit oscillatory CL zoning. However, the regularity of the oscillatory zoning does appear to vary between samples, with more regular (concentric and idiomorphic) oscillatory CL patterns observed in the larger quartz grains in the samples that were collected nearer to the centre of the sill. These observations are illustrated in Fig. 4, which shows representative CL images of quartz grains from the roof, centre and floor of the intrusion.

When focusing in on the larger quartz grains that form the multigrain quartz clusters in the centre of the intrusion for which there is also crystal orientation data (samples ZP131 & BBK1), it is common that one or both grains that share a CSL grain boundary exhibits a change in the regularity of oscillatory CL pattern (Fig. 5). This change in pattern regularity appears to always involve rounding of the annulus that forms one side of the CSL grain

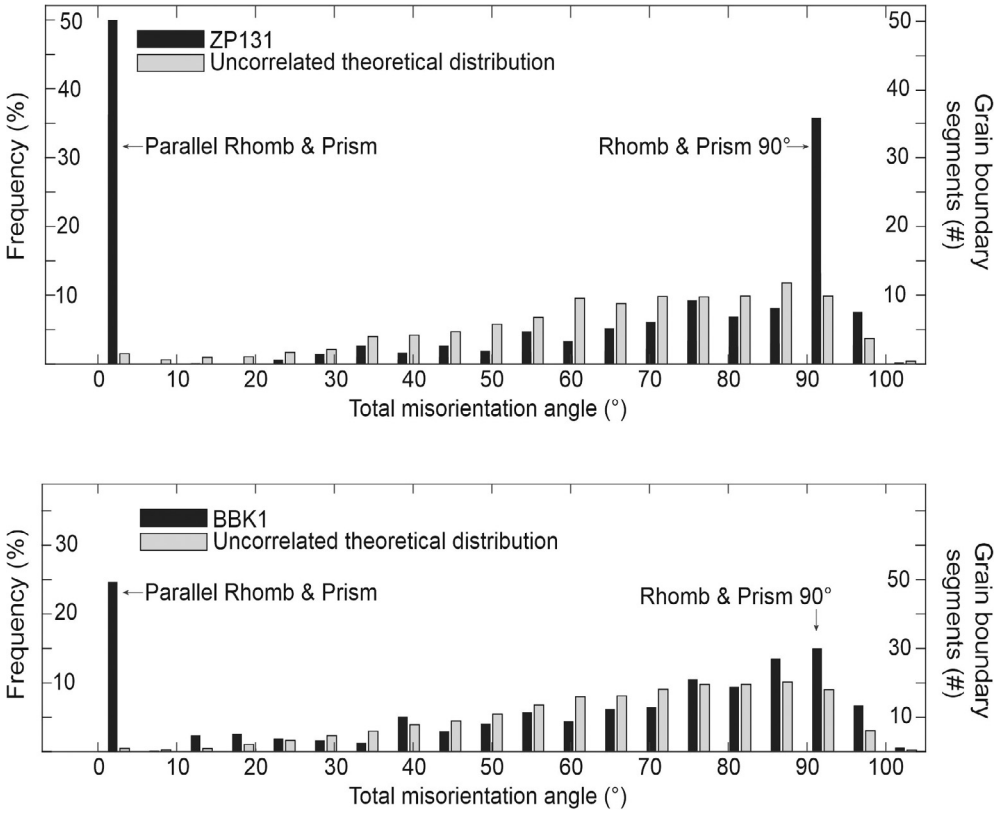

Fig. 2. Distribution of total misorientation angle for all measured grain boundary segments showing prominent peaks around angles predicted for attachment along parallel, prism 90°, and rhomb 90° orientation relationships. Note: parallel pairs identified in cathodoluminescence maps.

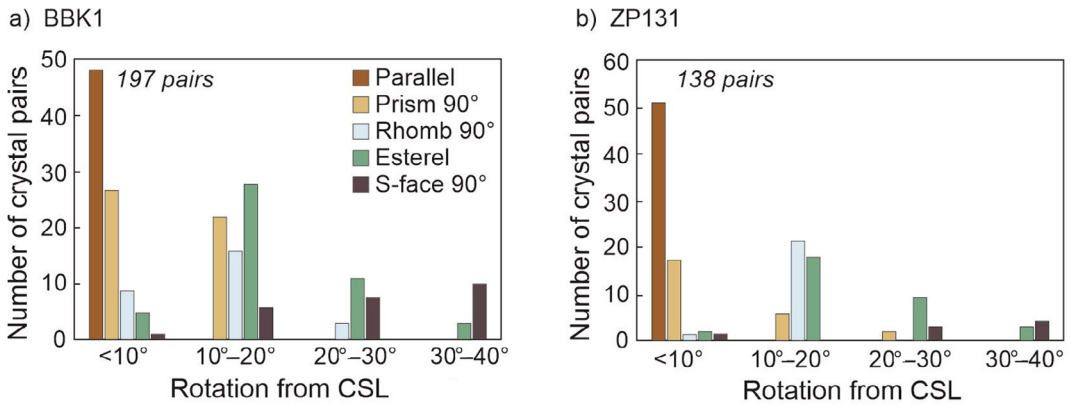

Fig. 3. (a) Number of crystal pairs in sample BBK1 observed at varying rotations from CSL. (b) Number of crystal pairs in sample ZP131 observed at varying rotations from CSL.

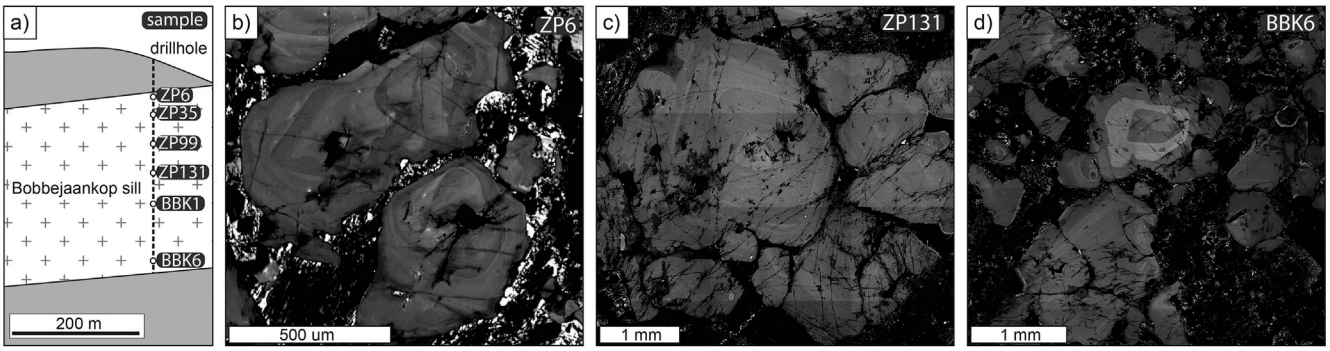

Fig. 4. (a) Schematic cross-section of the Bobbejaankop sill showing the stratigraphic position of samples studied, modified after Dyck and Holness (2022). Cathodoluminescence (CL) images of oscillatory zoned quartz from the (b) roof, (c) centre and (d) floor of the sill.

boundary (i.e., the outermost annulus during at the time of synneusis). The rounded boundary is identifiable by both a change in the curvature of the internal CL facets/zoning as well as the truncation of the previously formed (idiomorphic) oscillatory zonation found inward of the boundary. When comparing the variations in the CL patterns (e.g., the thickness and CL intensity) of the oscillatory annuli of sintered quartz pairs, there is a marked difference in the symmetry of zoning found inwards versus outwards of the rounded boundaries. Outwards of the rounded boundaries, both grains of a pair exhibit symmetrical CL zoning patterns (e.g., Fig. 5c). While there may be differences in the thickness of concentric annuli between grains, the sequence of CL intensities observed outwards of the rounded boundaries remains the same. This is, however, not the case when looking inwards of the rounding boundaries where there is generally no common sequence of CL zonation between the two grains of a sintered pair (e.g., Fig. 5e). The observed CL patterns implies that two grains of a pair grew separately at the time that their cores formed, stuck together at a time corresponding to when the rounded boundary formed, and thereafter grew together.

There are no discernible differences in either the occurrence or appearance of the rounding of CL zoning as a function of the specific orientation relationship of the sintered pair (e.g., whether the pair forms a parallel versus 90° or Esterel relationship); examples of rounding are found in crystal pairs that form parallel rhomb, parallel prism, rhomb 90°, prism 90°, Esterel relationships (Fig. 5c–f). The rounding of internal CL zoning described here is distinguished from other perturbations to the regularity of CL zonation that are commonly observed near the rim of quartz grains, which are typically irregular (e.g., wavy or lobate; Fig. 5f) and are present in samples from all stratigraphic levels of the intrusion.

It is worth noting that as the rounding generally occurs towards the centre of the grain pairs, and the thin-sectioning of the complex cluster shapes does not cut through the cores of all grains, there are some grain pairs that do not exhibit rounding of the CL pattern. These pairs instead show broadly symmetrical CL patterns across their common grain boundary. Accordingly, the lack of rounding associated with some sintered pairs may be an artefact of sample preparation.

4. Discussion

The observable phenomena associated with grain sintering in solidifying systems can be divided into three main stages: i) formation and growth of a crystalline neck at the contact between the two grains, ii) rigid-particle motion (translation and rotation) of one or both sintered crystals, and iii) grain growth (Dake et al., 2016; Bouala et al., 2017; Kini and Chokshi, 2020). The driving force behind the microstructural modifications in both stages 1 and 2 is the reduction of the grain boundary energy (interface energy) of the aggregated crystals, whereas grain growth (stage 3) is driven by reduction in Gibbs free energy of the solidifying system. When two suspended crystals come into contact the total area of free surfaces is lowered by the formation of a single crystal/crystal boundary. Although the absolute change in grain boundary energy during this process depends on many factors (e.g., liquid/-solid phase compositions, crystal orientation, impurity chemicals along the interface) it is generally on the order of one-third that of the free surface of equal area (Exner and Arzt, 1990). Accordingly, it is energetically favourable to both develop and then widen the crystalline neck that forms upon contact. Indeed, rapid neck

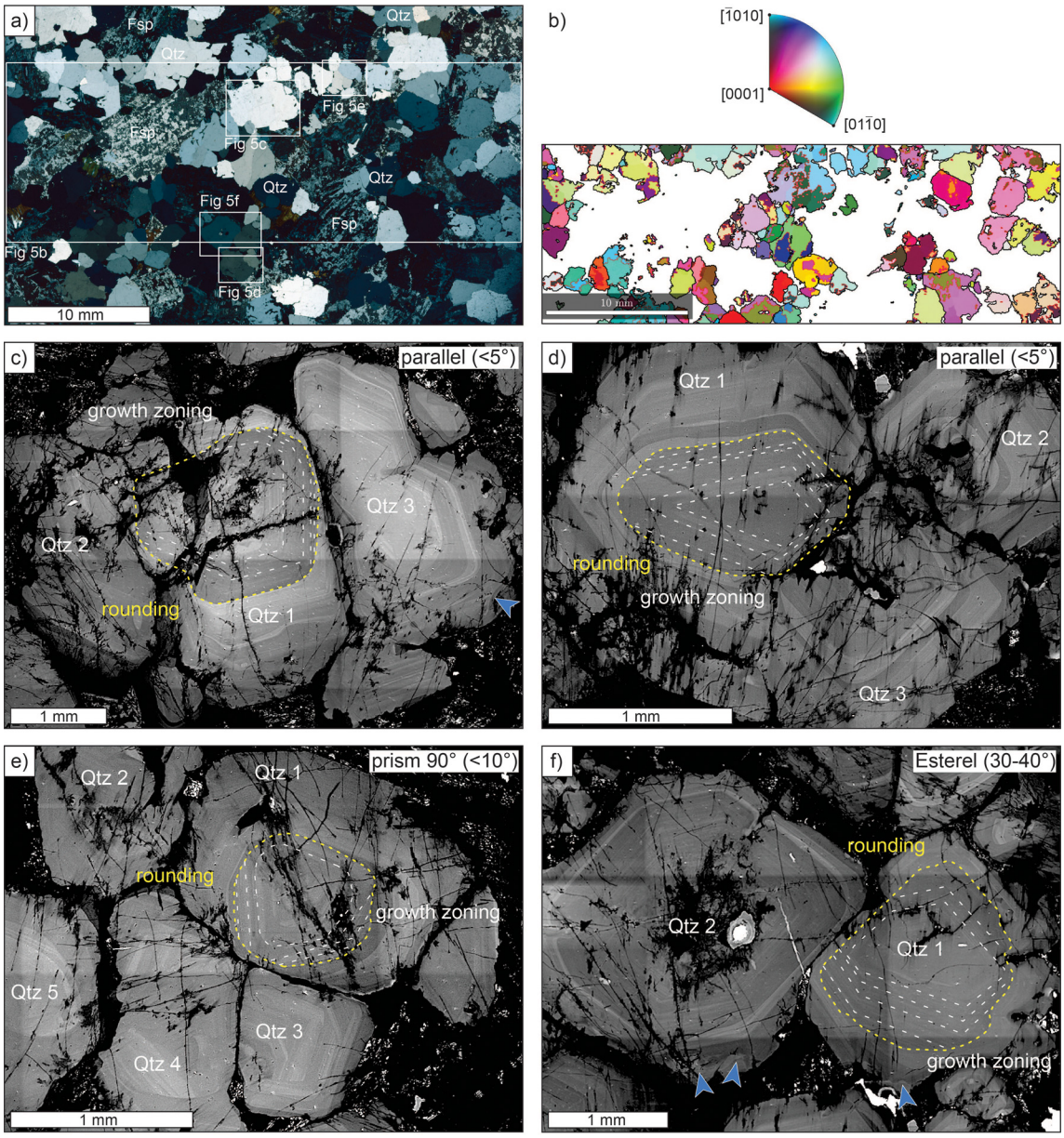

Fig. 5. Quartz (Qtz) microstructures in sample ZP131, collected from the centre of the sill. (a) Thin-section scan showing clustered quartz and feldspar (Fsp) under crossed-polars. (b) Quartz orientation map. (c–f) Cathodoluminescence (CL) images showing growth zoning (dashed white lines), rounding of oscillatory zoning (dashed yellow lines) and symmetrical zonation in rim overgrowths for quartz pairs formed at varying degree of rotation from the parallel, prism 90° and Esterel coincident site lattice orientation relationships. Blue arrows point to examples of the lobate CL patterns commonly observed near the rim of quartz grains. (For interpretation of the references to colour in this figure legend, the reader is referred to the web version of this article.)

growth has been observed in electron microscopy sintering experiments with both ThO_2 and Au microspheres (Nakaso et al., 2002; Bouala et al., 2017). Such microstructural modifications are accompanied by similarly rapid changes in crystal size and shape, enabled by the diffusion of components along the crystal surface. A common feature of models that describe crystalline neck growth is a surface motion driven by surface curvature, which is a difficult and challenging mathematical problem (Cahn et al., 1996). The governing equations are nonlinear time-dependent partial differential equations that are parabolic in nature such that the rate at which the neck radius grows is initially very rapid and decreases exponentially (Zhang and Gladwell, 1998). Based on the frequency of sintered quartz clusters found in high-silica granite I infer that the grain shape modification processes associated with neck growth operates on shorter timescales than those that relate to the movement of suspended crystals.

In a fully crystallized plutonic rock, where the porosity approaches zero, the crystal necks formed between sintered grains are not as readily observable as they are in crystal/liquid (or quenched glass) mixtures. However, as outlined below, the CL response and crystal orientations of the quartz clusters studied here preserve a record of microstructural modification and growth that is consistent with the three phenomenological stages of material sintering.

4.1. Stage 1: Binding of crystals by rapid neck growth

The idiomorphic, concentric, and oscillatory nature of the CL zonation observed in majority of the quartz core domains documented here is consistent with growth as isolated crystals suspended in melt (Alexandrov, 2001; Holness, 2018). That the observed rounding of quartz CL zonation consistently involves

the annulus that forms one side of the CSL grain boundary is a good indication that the 'rounding event' is associated with the initial pairing of the crystals. These rounding events are interpreted here as the preserved record of sintered neck formation and the attendant microstructural modifications that affect one or both of the sintered grains. The crystal rounding is a result of the preferential growth of the sintered neck width at the expense of the higher energy quartz–melt crystal surfaces. As with sintered alloys and ceramics (e.g. Nakaso et al., 2002; Kini and Chokshi, 2020), the growth of sintered necks may bind quartz crystals together and significantly increases the shear strength of the clustered grains.

In addition to the modification associated with synneusis, the observed rounding of quartz CL zoning may reflect a decrease in the rate of quartz growth following synneusis; a consequence of reducing the crystal/melt surface area. If quartz growth is temporarily slowed or paused, the crystals may transform towards their near-spherical quartz–melt equilibrium shape (Laporte, 1994). It is, however, unlikely that a decreased quartz growth rate alone would result in the observed rounding features because the rates of crystal-melt microstructural modification, while poorly constrained, are thought to be orders of magnitude slower than the relatively rapid grain shape modification associated with sintered neck growth (Ryan et al., 2020).

4.2. Stage 2: Rotation of crystals towards lower energy orientation relationships

Two mechanisms may have contributed to the high frequency of quartz-quartz pairs observed at <20° misorientation from CSL (Fig. 3). The first is that the success of quartz–quartz attachment may itself be a function of the degree of misorientation from CSL, with lower misorientations resulting in a higher probability of synneusis. There is a known dependence of grain boundary energy on the crystallographic misorientation of crystal pairs such that the grain boundary energy increases with increasing misorientation from CSL (e.g., Grupp et al., 2011). This dependency was aptly demonstrated by the rotating crystallite experiments of Chan and Balluffi (1985, 1986), where gold nanoparticles welded to a gold substrate rotated towards CSL upon heating, driven by a reduction in grain boundary energy. In a magmatic environment where suspended quartz crystals can move independently of each other, it may be that out of the many possible randomly oriented quartz–quartz collisions only the few that are near CSL result in synneusis. It may also be the case that the same hydrodynamic forces that bring crystals together also cause random grain rotations (with axes normal to quartz–quartz grain boundaries), which upon rotation to the lower-energy CSL orientation relationships are frozen in place.

The second and preferred way of interpreting the crystal orientation data presented here is that upon meeting along common crystal faces (i.e. rhomb–rhomb), quartz crystals rotate towards the lower-energy CSL orientation relationships. When a grain rotates, the energy along its surfaces will change and, when this rotation reduces the net misorientation with neighbouring crystals, interfacial energy is reduced (Wheeler et al., 2001). Accordingly, the torque required for rotation is driven by a reduction in grain boundary energy, and the magnitude of torque decreases as a grain pair approaches CSL. Molecular dynamic simulations demonstrate that individual grains in solid-state polycrystalline aggregates will undergo rotation towards local minima in grain boundary energy versus misorientation plots (Braginsky et al., 2005; Upmanyu et al., 2006). Although grain rotation does not require crystal suspension, rotation is more difficult to accomplish in a solid matrix and generally involves the mobility of grain boundaries that accompanies grain growth and shrinkage (Upmanyu et al., 2006; Trautt and Mishin, 2012, 2014). Whereas, the efficiency of grain rotation is greater when crystals are suspended in a liquid phase. This phenomenon is not restricted to nanoscale; Dake et al. (2016) report direct observations of grain rotations driven by grain boundary misorientation energetics on partially molten Al-Cu alloys (crystal fraction of 0.7) with grain diameters in excess of 200 μm. Similarly, experiments by Grupp et al. (2011) using tightly packed monocrystalline Cu spheres (80–100 μm diameter) resulted in the rotation of individual crystals by up to 8° from pre-sintering orientations. Further, Ohfuji et al. (2005) document the preferential alignment of pyrite crystallites in framboid clusters and interpret grain rotation as being the cause of the non-random disorientation distributions.

Grain boundary energy for silicates and alloys increases non-linearly from near zero at low misorientations (<0.1°) to ~1 J/m^2 at misorientations of ~10°–15°, above which the grain boundary energy takes on an approximately constant value (Duyster and Stöckhert, 2001; Dake et al., 2016). The precipitous drop-off in grain boundary energy below misorientations of ~15° may explain why (i) the majority of the quartz-quartz crystal pairs studied here were found to be within 0–20° of rotation from one of the prism or rhomb CSL orientation relationships, and (ii) for non-parallel CSL orientation relationships, fewer crystal pairs were observed at rotations of 0–10° from CSL than at rotations of 10°–20°. It may be that the torque required to rotate crystals towards CSL was insufficient at lower misorientation angles (e.g., <10°) and grain rotation stalled before reaching these orientations.

The formation of a crystal/crystal contact is a prerequisite for boundary energy-driven grain rotation. Therefore, grains may rotate at the same time that they are growing sintered necks. Accordingly, it may be that the rounding events preserved in the CL zoning reflects a combination of both the microstructural modifications associated with neck growth and with grain rotation.

4.3. Stage 3: Continued crystal growth

Following the attachment and alignment of quartz pairs along their shared grain boundaries there is a record of continued quartz growth. This growth resulted in identical CL patterns formed outwards of the synneusis boundary, reflecting a shared growth history after the crystals were joined (e.g., Fig. 5c). It is worth noting that clusters with multiple cores but a common overgrowth (visible as CL bands) can represent sections through twins or epitaxial overgrowths (Dowty, 1980). However, as demonstrated in Dyck and Holness (2022), both of those interpretations can be ruled out with complementary orientation data showing the clusters are made up of multiple independent grains.

5. Conclusions

Crystalline neck growth and post-attachment rotation of sintered crystals are two mechanisms that, while well-documented in alloy and ceramic studies, have largely been overlooked in geological studies. Together, these two mechanisms reduce the grain boundary energy of crystal clusters while increasing the cluster's shear strength. The continued crystallization of sintered phases (i.e. crystal growth outwards of the synneusis contact) will further act to cement the crystal pairs and resist disaggregation. Quartz is just one of many magmatic phases that forms clusters. However, the high-fidelity record of CL zoning in quartz provides particularly valuable insights into the growth and microstructural histories of sintered crystal, insights that should also apply to olivine, plagioclase and other phases that form magmatic clusters. Independent records of these processes may be revealed in the distribution of phosphorus in olivine (owing to its relatively slow diffusion), CL

zoning in plagioclase, and the crystal pair orientation relationships of crystal clusters.

Data Availability

All data and code underlying this article are available in the online supplementary material file and stored in the Open Science Framework online repository at: https://osf.io/em35q/?view_only=a404f05247164c9186371a5105a229a8.

Declaration of Competing Interest

The author declares that they have no known competing financial interests or personal relationships that could have appeared to influence the work reported in this paper.

Acknowledgements

I thank Associate Editor Dr. Richard Palin for handling this submission, Laurence Robb for loaning me the Bobbejaankop samples, and Marian Holness, George Bergantz and John Faithfull for the discussions that spurred on this paper. Helpful comments from three anonymous reviewers improved this manuscript. This work was supported by a NSERC Discovery Grant.

Appendix A. Supplementary data

Supplementary data to this article can be found online at https://doi.org/10.1016/j.gsf.2022.101512.

References

Alexandrov, P., 2001. Synneusis of zircon: why not? Mineral. Mag. 65, 71–79.
Bachmann, F., Hielscher, R., Schaeben, H., 2010. Texture analysis with MTEX–free and open source software toolbox. Solid State Phenom. 160, 63–68.
Beane, R., Wiebe, R.A., 2012. Origin of quartz clusters in Vinalhaven granite and porphyry, coastal Maine. Contrib. Miner. Petrol. 163, 1069–1082.
Bergantz, G.W., Ni, J., 1999. A numerical study of sedimentation by dripping instabilities in viscous fluids. Int. J. Multiph. Flow. Elsevier 25, 307–320.
Bouala, G.N., Clavier, N., Léchelle, J., Monnier, J., Ricolleau, C., Dacheux, N., Podor, R., 2017. High-temperature electron microscopy study of ThO2 microspheres sintering. J. Eur. Ceram. Soc. 37, 727–738.
Braginsky, M., Tikare, V., Olevsky, E., 2005. Numerical simulation of solid state sintering. Int. J. Solids Struct. 42, 621–636.
Cahn, J.W., Elliott, C.M., Novick-Cohen, A., 1996. The Cahn-Hilliard equation with a concentration dependent mobility: motion by minus the Laplacian of the mean curvature. Eur. J. Appl. Math. 7, 287–301.
Chaim, R., 2012. Grain coalescence by grain rotation in nano-ceramics. Scr. Mater. 66, 269–271.
Chan, S.-W., Balluffi, R.W., 1985. Study of energy vs misorientation for grain boundaries in gold by crystallite rotation method—I. [001] twist boundaries. Acta Metall. 33, 1113–1119.
Chan, S.-W., Balluffi, R.W., 1986. Study of energy vs misorientation for grain boundaries in gold by crystallite rotation method—II. Tilt boundaries and mixed boundaries. Acta Metall. 34, 2191–2199.
Dake, J. M., Oddershede, J., Sørensen, H. O., Werz, T., Shatto, J. C., Uesugi, K., Schmidt, S., Krill, C. E., 2016. Direct observation of grain rotations during coarsening of a semisolid Al–Cu alloy. *Proc. Natl. Acad. Sci.* **113**, E5998–E6006.
Dowty, E., 1980. Crystal growth and nucleation theory and the numerical simulation of igneous crystallization. In: Hargraves, R.B- (Ed.), Physics of Magmatic Processes. Princeton University Prcss, Princeton, New Jersey, pp. 419–485.
Duyster, J., Stöckhert, B., 2001. Grain boundary energies in olivine derived from natural microstructures. Contrib. Miner. Petrol. 140, 567–576.
Dyck, B., Holness, M., 2022. Microstructural evidence for convection in high-silica granite. Geology. Geological Society of America 50, 295–299.
Exner, H.E., Arzt, E., 1990. Sintering processes. Sintering Key Papers, 157–184.
Gardiner, N.J., Hawkesworth, C.J., Robb, L.J., Mulder, J.A., Wainwright, A.N., Cawood, P.A., 2021. Metal anomalies in zircon as a record of granite-hosted mineralization. Chem. Geol. 585, 120580.
Gogoi, B., Saikia, A., 2018. Synneusis: does its preservation imply magma mixing? Mineralogia 49, 99–117.
Grupp, R., Nöthe, M., Kieback, B., Banhart, J., 2011. Cooperative material transport during the early stage of sintering. Nat. Commun. 2, 1–6.
Hansen, L.N., Warren, J.M., 2015. Quantifying the effect of pyroxene on deformation of peridotite in a natural shear zone. J. Geophys. Res. Solid Earth 120, 2717–2738.
Holness, M.B., 2018. Melt segregation from silicic crystal mushes: a critical appraisal of possible mechanisms and their microstructural record. Contrib. Miner. Petrol. 173, 48.
Jerram, D.A., Cheadle, M.J., Philpotts, A.R., 2003. Quantifying the building blocks of igneous rocks: are clustered crystal frameworks the foundation? J. Petrol. 44, 2033–2051.
Kini, M.K., Chokshi, A.H., 2020. Initial stage sintering of polycrystalline spheres: A model and experiments. Materialia, 100665.
Laporte, D., 1994. Wetting behavior of partial melts during crustal anatexis: the distribution of hydrous silicic melts in polycrystalline aggregates of quartz. Contrib. Miner. Petrol. Springer 116, 486–499.
McIntire, M.Z., Bergantz, G.W., Schleicher, J.M., 2019. On the hydrodynamics of crystal clustering. Philos. Trans. R. Soc. A 377, 20180015.
Nakaso, K., Shimada, M., Okuyama, K., Deppert, K., 2002. Evaluation of the change in the morphology of gold nanoparticles during sintering. J. Aerosol. Sci. 33, 1061–1074.
Nazari-Dehkordi, T., Robb, L., 2022. Zircon mineral chemistry and implications for magmatic-hydrothermal evolution of the granite-hosted Zaaiplaats Sn deposit, Bushveld Large Igneous Province, South Africa. Lithos 416, 106672.
Ohfuji, H., Boyle, A.P., Prior, D.J., Rickard, D., 2005. Structure of framboidal pyrite: An electron backscatter diffraction study. Am. Mineral. 90, 1693–1704.
Oyegbile, B., Ay, P., Narra, S., 2016. Flocculation kinetics and hydrodynamic interactions in natural and engineered flow systems: A review. Environ. Eng. Res. 21, 1–14.
Robb, L.J., Freeman, L.A., Armstrong, R.A., 2000. Nature and longevity of hydrothermal fluid flow and mineralisation in granites of the Bushveld Complex, South Africa. Earth Environ. Sci. Trans. R. Soc. Edinb. 91, 269–281.
Ruggles, T.J., Rampton, T.M., Khosravani, A., Fullwood, D.T., 2016. The effect of length scale on the determination of geometrically necessary dislocations via EBSD continuum dislocation microscopy. Ultramicroscopy 164, 1–10.
Ryan, A.G., Russell, J.K., Heap, M.J., Zimmerman, M.E., Wadsworth, F.B., 2020. Timescales of porosity and permeability loss by solid-state sintering. Earth Planet. Sci. Lett. 549, 116533.
Trautt, Z.T., Mishin, Y., 2012. Grain boundary migration and grain rotation studied by molecular dynamics. Acta Mater. 60, 2407–2424.
Trautt, Z.T., Mishin, Y., 2014. Capillary-driven grain boundary motion and grain rotation in a tricrystal: a molecular dynamics study. Acta Mater. 65, 19–31.
Upmanyu, M., Srolovitz, D.J., Lobkovsky, A.E., Warren, J.A., Carter, W.C., 2006. Simultaneous grain boundary migration and grain rotation. Acta Mater. 54, 1707–1719.
Vance, J.A., 1969. On synneusis. Contrib. Miner. Petrol., Springer 24, 7–29.
Vance, J.A., Gilreath, J.P., 1967. The effect of synneusis on phenocryst distribution patterns in some porphyritic igneous rocks. Am. Mineral. 52, 529–536.
Walraven, E., 1993. Geochronology of the Nebo granite, Bushveld complex. S. Afr. J. Geol. 96, 31–41.
Wheeler, J., Prior, D., Jiang, Z., Spiess, R., Trimby, P., 2001. The petrological significance of misorientations between grains. Contrib. Miner. Petrol., Springer 141, 109–124.
Wieser, P.E., Vukmanovic, Z., Kilian, R., Ringe, E., Holness, M.B., Maclennan, J., Edmonds, M., 2019. To sink, swim, twin, or nucleate: A critical appraisal of crystal aggregation processes. Geology 47, 948–952.
Zhang, W., Gladwell, I., 1998. Sintering of two particles by surface and grain boundary diffusion–a three-dimensional model and a numerical study. Comput. Mater. Sci 12, 84–104.
Zhu, Y.-X., Wang, L.-X., Ma, C.-Q., Zhang, C., 2018. A flower-like glomerophyric diorite porphyry from Central China: Constraints on the unusual texture. Lithos 318, 1–13.